Substrate mimicry in the active center of a mammalian α-amylase: Structural analysis of an enzyme-inhibitor complex

ARTICLE *in* STRUCTURE · JANUARY 1997

Impact Factor: 5.62 · DOI: 10.1016/S0969-2126(96)00151-7 · Source: PubMed

4 AUTHORS, INCLUDING:

Coralie Bompard
Université des Sciences et Technologies de Li…
30 PUBLICATIONS **820** CITATIONS
SEE PROFILE

Pierre Rougé
Paul Sabatier University - Toulouse III
263 PUBLICATIONS **6,001** CITATIONS
SEE PROFILE

Substrate mimicry in the active center of a mammalian α-amylase: structural analysis of an enzyme–inhibitor complex

Coralie Bompard-Gilles[1], Patrice Rousseau[2], Pierre Rougé[2] and Françoise Payan[1]*

Background: α-Amylases catalyze the hydrolysis of glycosidic linkages in starch and other related polysaccharides. The α-amylase inhibitor (α-AI) from the bean *Phaseolus vulgaris* belongs to a family of plant defence proteins and is a potent inhibitor of mammalian α-amylases. The structure of pig pancreatic α-amylase (PPA) in complex with both a carbohydrate inhibitor (acarbose) and a proteinaceous inhibitor (Tendamistat) is known, but the catalytic mechanism is poorly understood.

Results: The crystal structure of pig pancreatic α-amylase complexed with α-AI was refined to 1.85 Å resolution. It reveals that in complex with PPA, the inhibitor has the typical dimer structure common to legume lectins. Two hairpin loops extending out from the jellyroll fold of a monomer interact directly with the active site region of the enzyme molecule, with the inhibitor molecule filling the whole substrate-docking region of the PPA. The inhibitor makes substrate-mimetic interactions with binding subsites of the enzyme and targets catalytic residues in the active site. Binding of inhibitor induces structural changes at the active site of the enzyme.

Conclusions: The present analysis reveals that there are extensive interactions between the inhibitor and residues that are highly conserved in the active site of α-amylases; α-AI1 inactivates PPA through elaborate blockage of substrate-binding sites. It provides a basis to design peptide analogue inhibitors. α-Amylase inhibition is of interest from several points of view, for example the treatment of diabetes and for crop protection.

Addresses: [1]AFMB-IBSM-CNRS, 31 Chemin Joseph, Aiguier 13402, Marseille, CEDEX 20, France and [2]Institut de Pharmacologie et de Biologie Structurale, UPR 9062, 205 Route de Narbonne, 31077 Toulouse, CEDEX, France.

*Corresponding author.
E-mail: fran@afmb.cnrs-mrs.fr

Key words: acarbose, α-amylase, bean inhibitor, Tendamistat, X-ray structure

Received: 2 July 1996
Revisions requested: 27 July 1996
Revisions received: 19 September 1996
Accepted: 10 October 1996

Structure 15 December 1996, 4:1441–1452

Introduction

α-Amylases (α-1,4-glucan-4-glucanohydrolases) are a group of enzymes widely distributed in microorganisms, plants and animal secretions. They catalyse the hydrolysis of the α-(1,4) glycosidic linkages found in starch components, glycogen and various oligosaccharides. Porcine, human, mouse and rat pancreatic α-amylases have a high degree of homology in their amino acid sequences [1].

The three dimensional molecular model of porcine pancreatic α-amylase (PPA) has been described in detail [2]. Subsequently, its interactions with a carbohydrate inhibitor (acarbose) were defined by the determination of the structure of the PPA–acarbose complex at 2.2 Å resolution, which showed a number of structural differences between the unliganded and liganded enzyme [3]. Recently, the structure of PPA in complex with the microbial inhibitor Tendamistat (74 amino acid residues), which belongs to the class of proteinaceous inhibitors from Streptomyces, has been reported [4]. This study shows that a segment of the inhibitor structure binds into the enzyme catalytic cleft, but a single one of the predicted catalytically competent residues, Glu233, is targeted by the inhibitor. The structural changes observed in the PPA–acarbose complex [3] were not detected in the active site of the PPA–Tendamistat complex structure.

Further structural information is required to increase our knowledge of PPA's function. The mechanism of enzyme inhibition by the widely occurring natural inhibitors is particularly unclear.

A number of proteinaceous inhibitors of α-amylases have been characterized in higher plants and microorganisms [5]. The seeds of the common bean, *Phaseolus vulgaris*, were shown to contain a family of plant defence proteins comprising phytohaemagglutinin (PHA), arcelin (ARL) and α-amylase inhibitor (α-AI) [6]. These three proteins have different functions, protecting seeds from being digested by mammals or infested by bruchid larvae that burrow into them.

α-AI inhibits the α-amylase in the digestive tract of mammals and coleoptera [7]. Recently, it was shown that when α-AI is expressed in a transgenic pea plant it inhibits the growth of certain bruchid larvae [8]. Two forms of the

α-amylase inhibitor have been described, α-AI1 and α-AI2 [9,10], which differ both in primary sequence and in their inhibitory activity towards bruchids. α-AI1 predominantly occurs in common bean seeds. A comparison of the amino acid sequences of lectins (PHA and *Lathyrus ochrus* Isolectin I [LoLI]) from the vetch *L. ochrus* and lectin-like proteins (ARL and α-AI1) from *P. vulgaris* shows that all four sequences have a high degree of both identity and homology. It is evident, however, that the loops involved in the carbohydrate-binding sites of lectins are absent in ARL and α-AI1 [11].

α-AI1 strongly inhibits PPA [7,12] ($K_d = 3.5 \times 10^{-11}$ M at neutral pH), but the pro-form is inactive until it is proteolytically processed at Asn77 [13]. Post-translational modification produces the active inhibitor (I) formed by the noncovalent association of two polypeptide chains (α and β) of 77 and 146 amino acid residues, respectively. Our preliminary structural analysis of the PPA–α-AI1 complex shows that it consists of a dimer of the inhibitor (I_2) and two molecules of the enzyme (E_2) in the crystal (total molecular weight 150 kDa) [14].

We describe here the structure of the complex between PPA and α-AI1 at 1.85 Å resolution. It reveals that there are extensive interactions between the inhibitor and the enzyme's active-site region. The interactions between α-AI and PPA directly mimic the protein–carbohydrate interactions observed in the PPA–acarbose complex [3].

Results and discussion

Structure of *phaseolus vulgaris* α-amylase inhibitor.

The overall architecture of the bean-inhibitor corresponds to a classical lectin fold (Fig. 1). The structure is devoid of α-helices and contains an abundance of antiparallel β sheets. In the crystal, two monomers (molecular weight 22.5 kDa) each consisting of a concave 12-stranded antiparallel β sandwich fold are associated by a twofold symmetry axis to create an extended β sheet with the enzyme combining sites at the two far ends of the dimer. The β-sheet-type hydrogen bonds between mainchain atoms of the strands adjacent to and related by the twofold axis seen in the legume lectin dimer are conserved in the α-AI1 dimer. When comparing the tertiary structures of LoLI [15] (226 residues) and α-AI1 (204 residues), 133 equivalent Cα atoms superimpose with a root mean square (rms) coordinate deviation of ~0.5 Å. Differences between the structures are confined primarily to the loop regions (Fig. 1) and appear to be related to the different carbohydrate-binding specificities of the two proteins. It is noteworthy that in the α-AI1 structure, two lectin carbohydrate-binding site loops (from residues 99–113 and 125–134; the numbering refers to the LoLI sequence [11]) are truncated. If present, these loops would overlap with a region of the enzyme structure (residues 145–157). A third loop, L2, (residues Ala209 and Glu210 of the lectins monosaccharide-binding site) is significantly longer in the inhibitor structure. The extended loop of α-AI1 interacts with the active site of PPA (Fig. 1); the lectin residue Glu210 superimposes with a inhibitor-residue involved in the enzyme–inhibitor interaction (Trp188, see hereafter). As shown on Figure 1, the carbohydrate/metal-binding site of lectins is located close to the enzyme-binding site. The processing site (Asn77) required for the activation of α-AI1 is located in the region where the carbohydrate-binding site occurs (around the lectin residue, Asp80), but in the present PPA–α-AI1 structure residues Gln75, Ala76 and Asn77 are not seen in the electron density.

This high-resolution study reveals three N-glycosylation sites at Asn12, Asn65 and Asn140 of each α-AI1 monomer. The two N-linked disaccharides on Asn12 and Asn65 are well ordered in the crystal, but for the branched carbohydrate projecting out from Asn140 there is no well

Figure 1

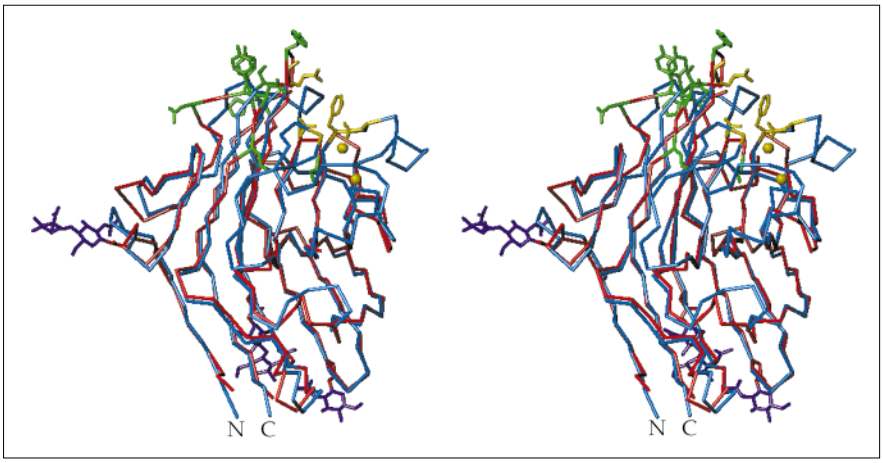

Stereoview of the α-carbon chain of the monomer unit of α-AI1 (red) superimposed on that of LoLI (blue) [15]. Metal ions and amino-acid sidechains involved in the lectin carbohydrate-binding site are coloured yellow, residues that interact with the active site of PPA are coloured green. Location of the three *N*-glycosylation sites is shown (the GlcNAc moieties are coloured purple).

defined electron density beyond the N-glycosyl linkage. The branched carbohydrate linked to Asn65 protrudes in the solvent, and is stabilized by the usual hydrogen bonds and hydrophobic interactions.

The most striking feature of α-AI1 is a branched disaccharide projecting out from Asn12. This residue is located on the segment connecting the first strand (part of the typical monomer–monomer interface of the legume lectin family) and a strand of the concave facing sheet. The two β-(1,4)-linked *N*-acetylglucosamine GlcNAc entities are found in a solvent channel that links the dimer to the enzyme, and adopt an extended conformation parallel to the surface of the dimer. They make direct or water-mediated hydrogen bonds with residues from the twofold related monomers (residues 12, 13 and 24 from one monomer and residues 170, 173 and 174 from the related monomer). These interactions make a significant contribution to the stability of the dimer assembly. Asn12 is not far from the inhibitor active site. The β strands of the hairpin loop (14–25) establish β-sheet-type hydrogen bonds with the main-chain atoms of adjacent strands of the parallel hairpin loop L1 (29–46), which in turn are hydrogen bonded to those of the hairpin loop L2 (171–189); L1 and L2 form part of the active site of the inhibitor (see below). The GlcNAc moieties identified here are not directly involved in the enzyme-inhibitor interaction, however.

Residues involved in α-AI1 binding to PPA

Contrary to earlier enzymological studies [16], the present structural analysis reveals that α-AI is dimeric and interacts with two pancreatic enzyme molecules (PPA). Kinetics measurements of the inhibition of PPA by α-AI1 (P Rousseau and P Rougé, unpublished data) support the idea that α-AI1 αβ units are themselves organized as dimers as seen in the crystal PPA–α-AI1 structure, and that the structure observed here is therefore biologically relevant.

In the present structure, each α-AI1 monomer (I) binds at the active site of an enzyme-molecule (E) (Fig. 2). The major interactions with PPA occur directly within the V-shaped depression of the active site, which also binds

Figure 2

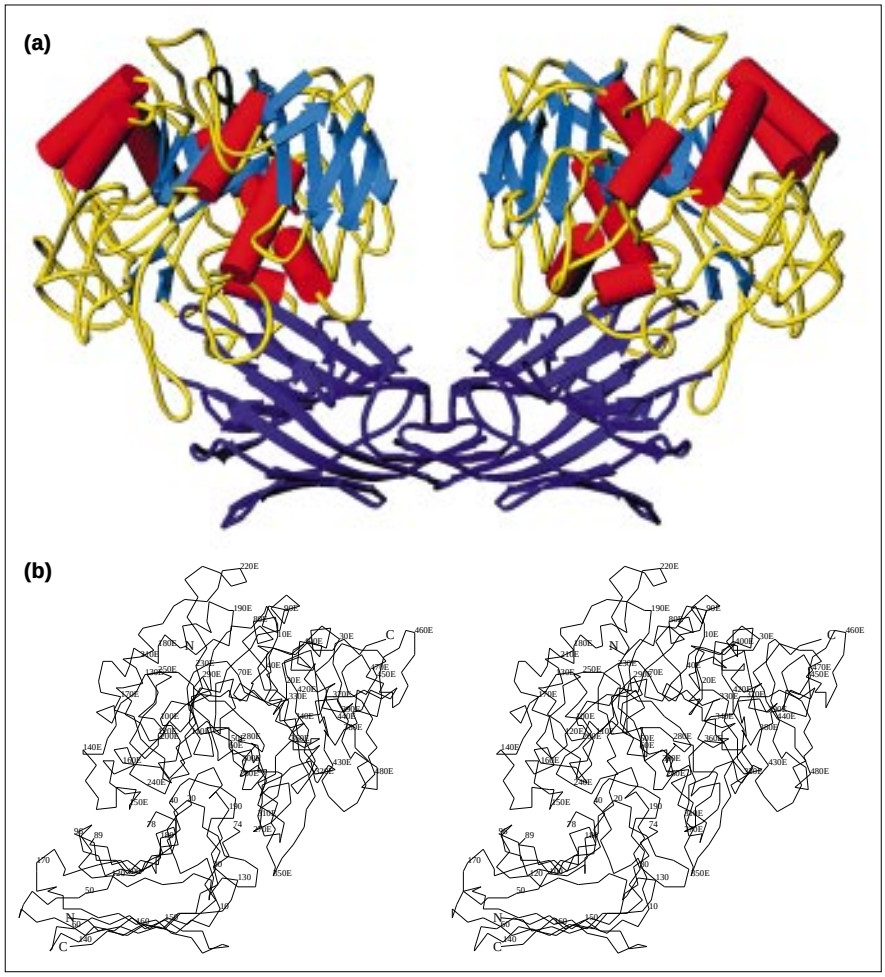

Structure of the PPA–α-AI1 complex
(a) Overall structure of the PPA–α-AI1 complex. PPA is shown with α-helices in red and β-strands in blue. Connecting loops are shown in yellow; α-AI1 is coloured purple.
(b) The chain-fold of the PPA–α-AI1 complex, given as Cα-backbone model. One monomer unit of α-AI1 in interaction with a molecule of PPA is shown. The residue numbers of PPA are followed by an 'E'. Figure was generated using TURBO-FRODO [32].

Figure 3

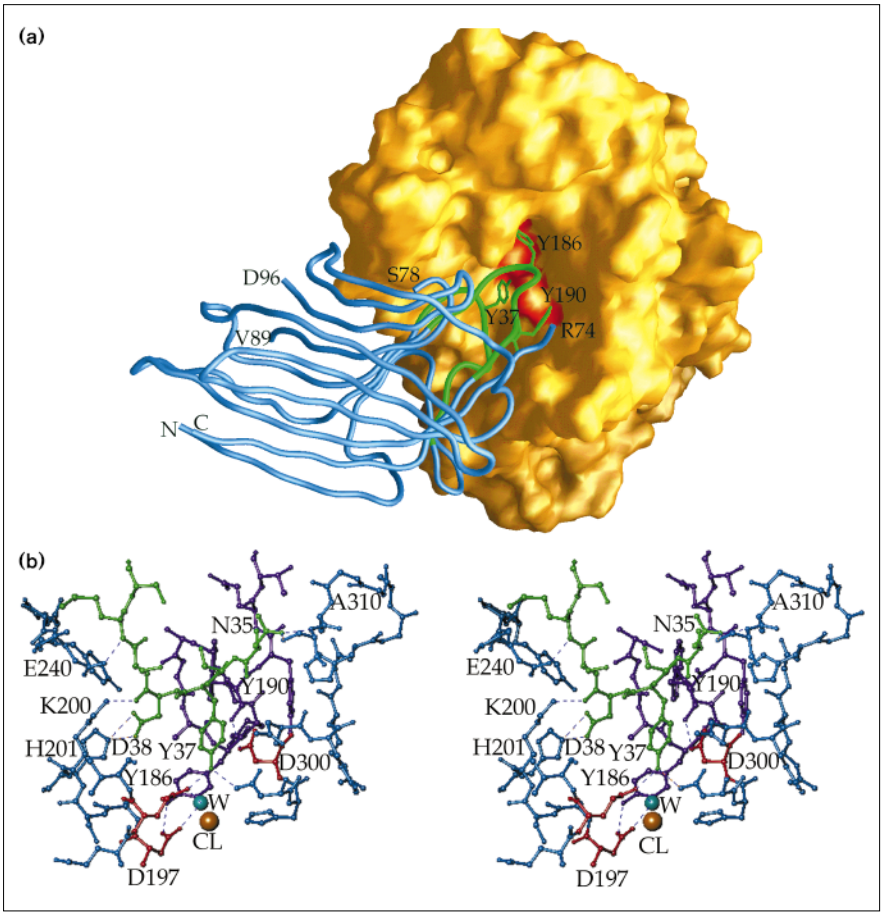

Residues involved in PPA–α-AI1 interactions. (a) Interaction of the two hairpin loops of the inhibitor with the substrate-binding cleft. The molecular surface of PPA is shown (gold). The deep polysaccharide binding cleft can be seen passing across the midsection of the enzyme. The mainchain of α-AI1 is represented by a blue tube, the two hairpin loops (L1 and L2) interacting directly with the active site are coloured green. The tyrosine sidechains (residues 37, 186 and 190), important to the interaction are depicted in a stick representation and PPA surfaces of the targeted catalytic residues are coloured red. The branches of the processed loop (R74; S78) can be seen at the top of the inhibitor model, on both sides of the green hairpin loops. (Figure was produced using GRASP [35].) (b) Detailed stereoview of a close up of sidechains involved in the complex formation. Shows the two hairpin loops (green and purple) of the inhibitor which insert into the active site of the enzyme, also shown (blue) are the amino acid residues of PPA involved in the interaction. The catalytically competent residues of the enzyme, Glu233, Asp300 and Asp197, are coloured red. In the immediate environment of the enzyme catalytic residues, the brown sphere represents the position of the chloride ion, the blue sphere indicates the water molecule W643, present in the free enzyme structure.

the carbohydrate inhibitor acarbose [3]. The inhibitor α-AI1 completely blocks one end of the enzyme cavity (the reducing end of the acarbose-ligand [3] and prevents the access to the other end through steric hindrance. The loops from domains B and A of the enzyme structure (notation according to Qian *et al.*, [2]), which build the walls of the V-shaped active-site cavity [3], make strong interaction with the inhibitory site of α-AI1.

The high-resolution studies of PPA complexed with the inhibitor acarbose [3,17] revealed in detail the arrangement of the protein residues related to six subsites of the active-site cleft. In the PPA–α-AI complex, two facing hairpin loops emerging from the β sheet fold, which consists of the stretches 29–46(I) in L1 and 171–189(I) in L2, lie fully in the active-site depression of PPA making extensive hydrogen-bonding, hydrophobic and water-bridged contacts with the enzyme active-site residues involved in PPA–acarbose interactions [3] (Fig. 3; Table 1). The conformation of the two functional hairpin loops is stabilized by hydrogen bonds occurring between mainchain atoms of the facing strands from the two loops. The presumed presence of a calcium ion (see hereafter) integrated into this structure, stitching together the two hairpin loops L1 and L2, contributes to the integrity of the inhibitor active site. Note this structural element brings together two loop regions which deviate widely from the corresponding loops of LoLI.

Regions located in the neighborhood of the enzyme active-site depression are also involved in the interactions with the inhibitor. An external convex segment from the domain B (residues 142–154(E)) interacts with a concave region of the inhibitor (Table 1). Similarly, a long loop corresponding to residues 349–357(E) from the domain A, which protrudes in to the solvent in close proximity to the flexible 303–309(E) loop [3], also participates in the interaction. The total buried surface area in the α-amylase inhibitor complex is about 3050 Å^2 (1461 Å^2 for PPA and 1588 Å^2 for the inhibitor), one of the largest reported values for a protein complex [18]. There are 50 residues from PPA and 40 residues from α-AI1 involved in the enzyme-inhibitor interface.

Conformational changes in the enzyme

Upon binding of α-AI1, the structural changes observed at the active site of the enzyme are very different from those induced by the carbohydrate inhibitor acarbose [3].

Table 1

Total contacts in the PPA–α-AI complex.

Amino acid residues*		Hydrogen bonds between PPA and α-AI atoms†	
Enzyme residues	Inhibitor residues	Direct hydrogen bonds	Water-mediated hydrogen bonds‡
Trp58, Trp59, Trp62	Tyr190, Gln187, Tyr186	–	–
His101	Tyr186	His101 Nε2↔Tyr186 OH	–
Ile148, Glu149, Ser150	Met40, Ser78, Ala79, Glu101	Glu149 O↔Ser78 N	Glu149 Oε1↔W44↔Asp117 Oδ2
Tyr151, Asn152, Asp153	Asn115, Asp117, Thr182	Tyr151 OH↔Asp38 Oδ1	Tyr151 N↔W758↔Ser78 O
Gln156			Tyr151 N↔W758↔Thr182 Oγ1
Leu162, Val163, Gly164,	Asp38, Phe105, Ala185		
Leu165	Tyr186, Trp188		Val163 N↔W694↔W8↔Ala79 O
Asp197, Ala198, Lys200,	Asp38, Ser39, Tyr186	Asp197 Oδ1↔Tyr186 OH	
His201		Lys200 Nζ↔Asp38 O	
		His201 Nε2↔Asp38 Oδ1	
		His201 Nε2↔Asp38 Oδ2	
Glu233, Ile235, Leu237	Gln20, Asp21, Ser36, Tyr37	Glu233 Oε1↔Tyr37 OH	Ile255↔W35↔Asp38 Oδ2
Gly239, Glu240, Phe256	Ser39, Met40	Glu240 Oε2↔Met40 N	Glu233 Oε2↔W82↔Asp38 Oδ2
			Glu233 Oε2↔W748↔W5↔Tyr186 N
			Leu237 N↔W690↔W27↔Met40 O
			Phe256 O↔W569↔W34↔Asn35 O
Asn298, Asp300, Arg303	Gln31, Tyr34, Asn35, Tyr37	Asn298 Nδ2↔Tyr37 OH	Gly304 O↔W2↔His73 Nε2
Gly304, His305, Gly308	His73, Tyr190	Asp300 O↔Tyr190 OH	His305 Nδ1↔W33↔Tyr34 O
Gly309, Ala310, Ser311		Asp300 Oδ2↔Ser189 Oγ	Gly309 O↔W83↔Gln31 Nε2
Ile312, Glu352		Ser311 N↔Asn35 Oδ1	Gly309 O↔W9↔Asn35 Nδ2
		Ser311 Oγ↔Asn35 Oδ1	Gly309 O↔W13↔W110↔Gln31 Nε2
		Glu352 Oε1↔His73 N	

*Contacts considered between 2.5 and 4 Å. †Contacts considered between 2.5 and 3.3 Å. ‡W refers to water molecule.

The flexible loop (residues 304–310(E)) which forms the surface edge of the substrate binding site was previously shown to move in toward the saccharide, thus reducing the cleft breadth. In contrast, when PPA is complexed with α-AI1, the same loop moves out toward the solvent, pushed away by the inhibiting entity which takes its place in the tight-binding inhibition process. The loop rotates outwards ~132° around an axis lying between Cα303 and Cα309. It should be noted that the sidechain of catalytic residue Asp300 which rotates ~60° around the Cα–Cβ bond upon acarbose binding, is found in the PPA–α-AI1 complex, in the same conformation as the free enzyme. The described conformational changes are accompanied by readjustment of the surrounding regions: the loop region including residues 351–359 (E) (domain A shows particularly large movements), the maximal mainchain movement being 6 Å (for Asn350). The fragment including residues 141–153 (E) from the domain B is also displaced, the maximal mainchain movement being 2 Å for Ala144. Displacement of the loops in response to the inhibitor binding can be seen in Figure 4.

As Wilcox and Whitaker [19] pointed out, inactivation of α-amylase by α-AI1 is slow; this may be caused by a requirement for a conformational change. The present data does indeed show large conformational changes in PPA structure upon α-AI1 binding.

In their structural analysis of the PPA–Tendamistat complex [4], the authors proposed a conformational change of α-amylase which would involve regions 305–310 and 57–61. Our studies ([2,3], this work and M Qian and FP, unpublished results) confirm that the region 304–309 corresponds to a moving loop able to adopt different conformations according to the ligand structure; however, the fragment of sequence 57–61 appears as a well defined region in the electron-density maps and it adopts the same conformation in free and all known complexed PPA structures.

Analysis of the inhibition scheme

In the structure of the PPA–α-AI complex, there is an extended protein–protein interface that might account for the large inhibition constant (K_i=3.5×10^{-11}); a similar feature was observed in the structure of PPA complexed with the proteinaceous inhibitor Tendamistat [4]. This extended protein–protein interaction by itself might inhibit the enzyme by sterically blocking the active-site cleft as observed in the structure of barley α-amylase in complex with the proteinaceous inhibitor Barley α-amylase/subtilisin inhibitor (BASI) [20]. However, analysis of the latter complex did not reveal any structural change or intimate enzyme–inhibitor contacts at the catalytic center. The active site of the plant α-amylase, complexed with BASI, appears to remain in the right conformation

Figure 4

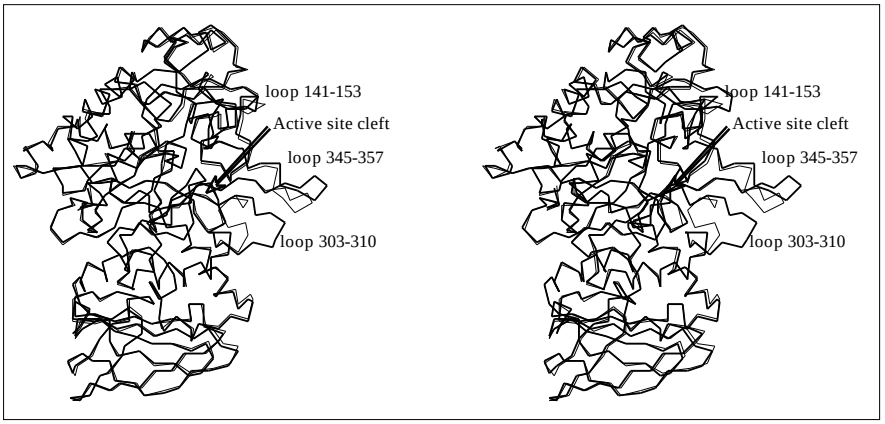

A stereoview of the superimposition of the α-carbon backbone traces of free and α-AI1 complexed PPA structures (see text). The thick lines correspond to the structure of the complexed enzyme.

to accept the ligands. In the mammalian complexes, in contrast, sidechains of inhibitor residues bind into the active-site cleft. They make strong interactions with the presumed catalytic residues, the chloride ligand and the surface edge of the catalytic depression formed by the flexible loop identified in Qian *et al.* [2,3]. It is thus clear that depending on the structure of the ligand, the moving loop adopts different conformations and strongly takes part in the ligand docking. This suggests that the motion of the active-site region is important for enzyme function and necessary to dock the various ligands. Therefore we suggest that in the intricate interaction pattern, strong contacts occurring within the active-site cleft are strictly associated with the extended protein–protein interaction in the mammalian enzyme inhibition.

As shown in Table 1, most of the inhibitor residues which form the binding segments of the complex are found in the two hairpin loops L1 and L2. In the structural analysis of the complex PPA–Tendamistat [4], it was observed that the loop region 304–309 (corresponding to the flexible loop characteristic of the mammalian α-amylases) binds residue Tyr15 of Tendamistat and therefore the authors suggested that position 15 in the proteinaceous inhibitors is important for strong interaction with mammalian α-amylases. In the present analysis, a substantial number of the residues from loop L1 and residue Tyr190 from loop L2 are engaged in interactions with the flexible loop. We therefore argue that these inhibitor elements are important in recognition and inhibition of mammalian α-amylases.

Comparison of the binding segments of PPA identified in the PPA–α-AI and PPA–Tendamistat complexes shows that the same main regions of PPA are involved in the tight contacts. In the present structure, however, 14 more enzyme residues are involved in the interaction, including in particular all the presumed catalytic residues (Asp197, Glu233, Asp300 and the chloride ligand Asn298), which are involved in hydrogen bonds with inhibitor residues (Tyr186, Tyr37 and Ser189). In the PPA–Tendamistat complex, a segment containing the staggered sidechains of the triplet Trp18, Arg19 and Tyr20 (typical for this class of inhibitors) binds into the catalytic site. Arg19 points out from a bulky head feature to form a salt bridge with Glu233, and Tyr20 is hydrogen bonded to His201 Nε2; in the present PPA–α-AI1 complex two hairpin loops lie completely in the active site and Tyr37, protruding from the extremity of L1, makes strong hydrogen bonds with the same catalytic residue Glu233 (and with the chloride ligand, Asn298) while the flanking residue Asp38 is hydrogen bonded to His201 Nε2. Another α-AI1 residue Tyr186 (I) sticks into the heart of the catalytic site, forming hydrogen bonds with the catalytic nucleophile Asp197 [21]. Asp300, the third residue of the presumed catalytic triad (Asp197, Glu233 and Asp300) is connected to Ser189(I) through its carboxyl oxygen and to Tyr190(I) through its carbonyl oxygen. A major feature observed in the PPA–Tendamistat complex is the bulky head of Tedamistat, containing six amino acids, (Tyr18, Arg19, Tyr20, Thr55, Gly59, Tyr60). It apparently forms hydrophobic contacts with the elements, also involved in the PPA–acarbose interaction (Trp58, Trp59, Tyr62, Tyr151, Leu162, Val163), lining the active-site depression [3]. This feature is also involved in the structure of α-AI1 complexed to PPA; in this case the inhibitor residues are: Ala185, Tyr186, Gln187, Trp188, Tyr190, Asp38 and Phe105 (Table 1). In this interaction, the sidechain of Gln187(I) stacks against the indole ring of Trp59(E) and the residues of the structural feature consisting of Tyr190, Gln187 and Tyr186 (I) form hydrophobic interactions with the aromatic residues Trp58, Trp59 and Tyr62 (E) (Fig. 5). From the published drawings [4] it appears that in the PPA–Tendamistat structure Trp18 is also parallel to the plane of Trp59 (E) and according to the analysis it is involved in hydrophobic interactions with the aromatic residues Trp58, Trp59 and Tyr62 (E). Additional hydrophobic interactions occur between Arg19 of Tendamistat and

Figure 5

Hydrophobic stacking features in the active-site depression. Thick lines correspond to the amino acid residues from the enzyme. The density is from a $2F_o–F_c$ SIGMAA-weighted [31] map contoured at 1σ.

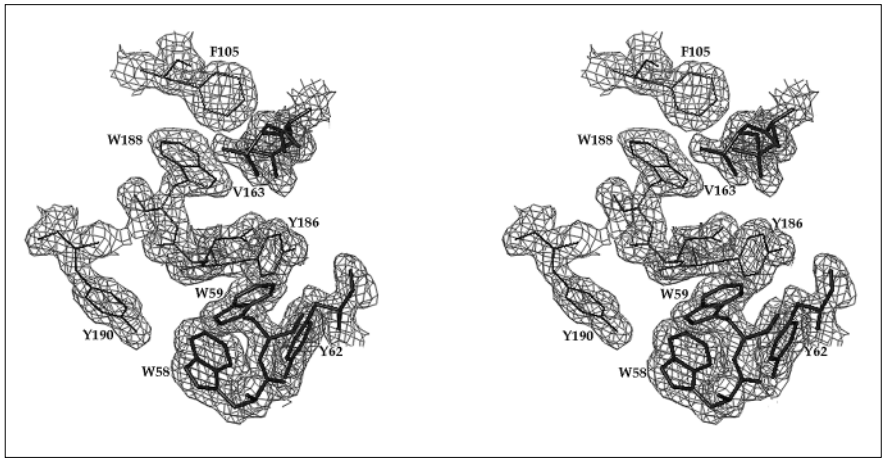

Val 163 of PPA; Tyr20 (Tendamistat) and Tyr151, Leu162, His201, Ile235 (E). In the PPA–α-AI1 structure the corresponding regions of PPA are principally involved in stacking with the inhibitor residues Phe105, Trp188 Tyr186, Tyr37 and Asp38; the residues Tyr20 (Tendamistat) and Asp38 (α-AI1) are apparently surrounded by the same PPA-residues (Tyr151, Leu162, His201, Ile235). According to the above observations, we propose that the triplet Trp18-Arg19-Tyr20 in Tendamistat corresponds to the sequence Tyr186-Gln187-Tyr190-Trp188-Tyr37-Asp38 in the bean inhibitor. Structural analyses of the mammalian complexes clearly indicate the important role of the aromatic residues lining the active site of the enzyme in recognition and binding of the ligand.

Protein-engineering studies [22] based on the structural analysis of the PPA–Tendamistat complex and a modeled structure of α-AI1, suggest that residues Trp188, Arg74 and Tyr190 of α-AI1 closely match the tripeptide sequence that forms the inhibitory region in the bacterial α-amylase inhibitor. These experiments led to the conclusion that the three residues constitute the active site of α-AI1. According to our data, Arg74 cannot have the role of Arg19 (in Tendamistat) namely that of interacting with a catalytic residue. In the present structure, the sidechain of Arg74 (in the area where the processing occurs) is not seen in the electron density and could hardly be modeled. In this region of the protein, there is no room for the sidechain of this residue. In the absence of any structural information, we are not able to speculate further on the total inactivation resulting from the replacement of Arg74 by asparagine [22]. However, according to the well defined electron-density map and the reasonable B factor values observed for residues Arg74 and Ser78, the absence of Gln75, Ala76 and Asn77 in the α-AI1 structure could result from the post-translational processing of the α-AI precursor. This is consistent with the fact that the surrounding residues Arg74 and Asn77 are susceptible to a proteolytic cleavage by a trypsin-like and an asparaginyl-endopeptidases enzymes respectively. A similar excision process was shown to occur during the post-translational maturation of the pea (*Pisum sativum*, PsA) lectin precursor to give the two-chain (β+α) lectin [23]. An excision event such as this might explain why a single mutation occurring at Arg74 would result in total inactivation of the α-AI inhibitor by preventing the natural proteolytic processing of the precursor, and not by directly affecting the PPA–α-AI1 inhibition process. As for the two other residues proposed as the active-site-binding residues (Trp188 and Tyr190), it is clear that Trp188(I) does not make any interaction with the catalytic residues, but as noted above, it is involved in stacking features with enzyme residues lining the entrance of the binding cleft. Further along the strand, the sidechain of residue Tyr190(I) forms strong contacts with the catalytic residue Asp300 (E) and is involved in hydrophobic contacts with the flexible loop (Table 1). These interactions constitute a possible explanation for the results of Mirkov *et al.* that showed that these residues are important for the activity of α-AI1 [22].

The observed structural arrangement suggests that the processing of the polypeptide at Asn77(I), which is necessary to activate the inhibitor, may induce a conformational change since the segment 73–74 of the inhibitor structure and particularly the segment 78–81 at the N terminus of the β subunit deviate from the corresponding lectin loop; the latter segment swings outwards, exposing and positioning residues that can then interact with the enzyme (Table 1; Fig. 3a). It appears that the uncleaved loop (as seen in the corresponding LoLI structure) would overlap with the sidechain of the inhibitor residue, Trp188. This might be related to earlier proposals suggesting that the polypeptide cleavage removes a conformational constraint on the precursor to produce the biochemically active molecule [13].

Figure 6

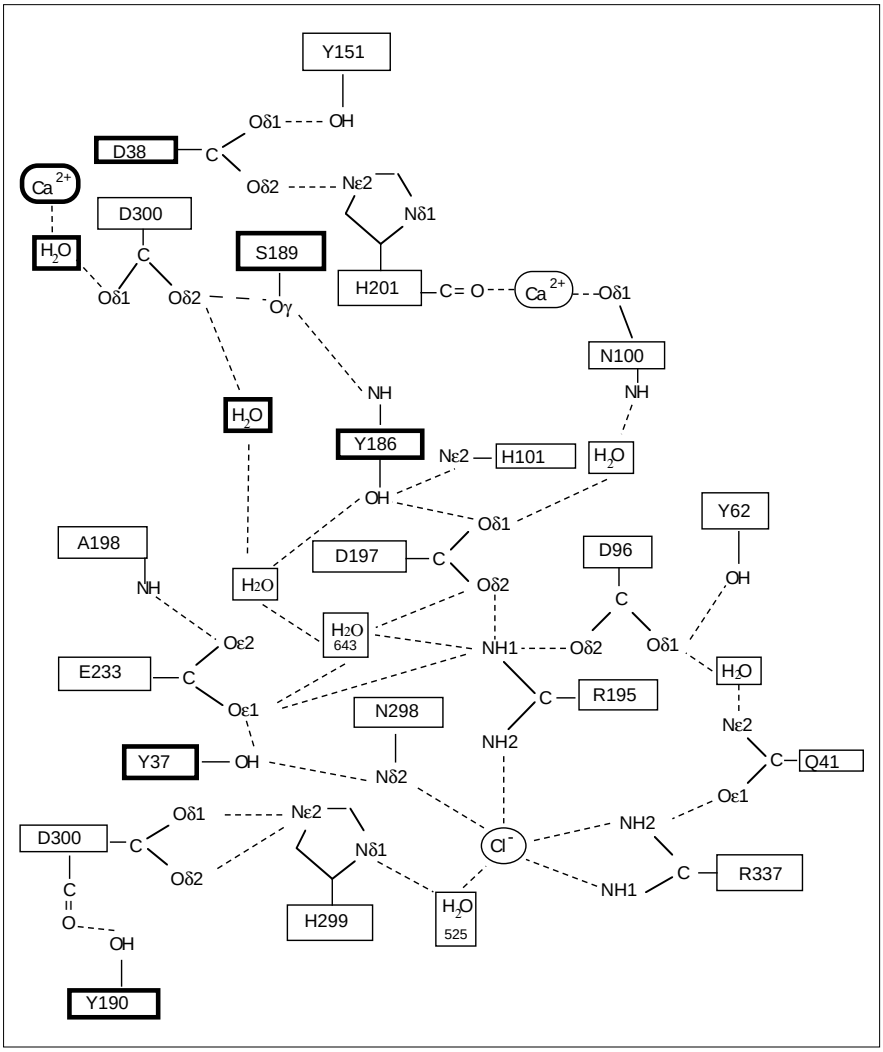

Schematic representation of the network of interactions within the catalytic center. The enzyme chloride ion is shown in interaction with some of its ligands (Arg195, Asn298 and H_20). The calcium ion of the enzyme structure (liganded to Asn100 and His201) and the presumed calcium ion of the inhibitor structure are involved in the interaction. (Borders around inhibitor residues are thickened.)

Comparison with the acarbose–PPA interaction

The X-ray crystal structures of the PPA–acarbose complexes [3,17] provide details of the relative disposition of atoms in the enzyme–carbohydrate-inhibitor interaction. They represent a subset of residues directly involved in binding the inhibitor and/or in a position to assist catalysis. In the catalytic center, the carboxylic oxygens of the catalytically competent residues Glu233 and Asp300 form hydrogen bonds with the 'glycosidic' NH group of the acarviosine moiety, and Asp197 lies on the opposite side of the inhibitor-binding cleft. After considering these crystallographic results, we proposed that both Asp197 and Glu233 are required to produce the β-linked glycosyl-enzyme intermediate. Recent results [21] clearly confirm the role of Asp197 as the catalytic nucleophile; Glu233 and Asp300 are hydrogen bonded to each other via an intervening water (W555) as well as to the glycosidic amine [3], and may be involved in acid/base catalysis.

The information derived from this structure, the structure of PPA in complex with the proteinaceous inhibitor α-AI1, is therefore strikingly different around the active-site cleft from that derived from previous α-amylase–inhibitor complexes.

The current structural analysis clearly shows intimate contacts between the bean inhibitor and the α-amylase catalytic residues (Figs 3b,6). The analysis of the present structure discloses that elements from the inhibitor molecule manage to fill the whole substrate-docking region of PPA producing interactions similar to the enzyme–carbohydrate-based-ligand interactions. These elements occupy the ligand-induced functional position of the enzyme residues required for binding and/or catalysis (Fig. 7).

The segments of β strands from the two inhibitor loops L1 and L2 follow the track of the flexible loop that form

Figure 7

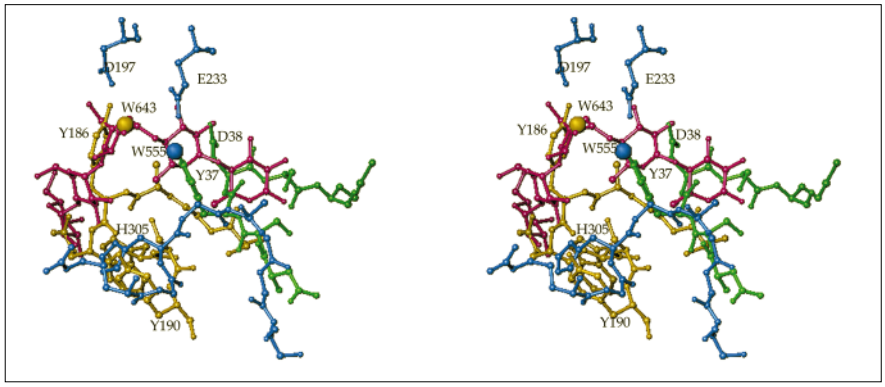

Substrate mimicry. Stereoview of the superimposition of α-AI1 peptide groups on the acarbose ligand (coloured pink) and 'flexible loop' (coloured blue) from the PPA–acarbose complex [3]. The loop L1 (coloured yellow) of α-AI1 mimics the closed position of the enzyme-flexible loop (blue) in the region that accommodates the reducing-end glucose (subsite 5). The part of the flexible loop involved in the architecture of the non-reducing end (subsites 2 and 1) is mimicked by the inhibitor segment from loop L2, coloured green. Also shown in blue are the catalytic residues Glu233(E) and Asp197(E), which interact with the inhibitor residues Tyr186 and Tyr37. Water molecule W555 (blue sphere; from the free and acarbose-complexed PPA structures) superimposes with the hydroxyl group of Tyr37(I). The yellow sphere corresponds to a water molecule W643 from the PPA–α-AI1 complex (see text).

the surface edge of the active site upon acarbose-ligand binding. Sidechains of residues from the strands run into the cleft and mimic the interactions between the sugar ligand and enzyme. In the present structure, Gln187(I) stacks against the indole ring of Trp59(E) as observed for the carbohydrate inhibitor's surface in subsite 1 and *2* [3]. A similar mimicry is produced by the hydrophobic sidechains of residues Trp188(I) and Phe105(I) stacking against the sidechains of residues Leu162(E) and Val163(E) (Fig. 5), which are known to stack against the acarbose surface in subsite 4. As noted above, these regions of the enzyme molecule also appear to mediate the hydrophobic contacts with the binding segments of inhibitor Tendamistat [4]. Residue Asp38(I) on the loop L1 completely occupies the subsite 5 and blocks the access to the region of the ligand-reducing end. Residue Try190 occupies the position of His305(E) in its functional position bound to the carbohydrate ligand (Fig. 7).

At the heart of the substrate-binding site, two tyrosine residues Tyr37(I) and Tyr186(I) (Fig. 3a,b), protruding from the extremity of the two hairpin loops L1 and L2 of α-AI1 combine to provide interactions with the presumed catalytic residues of the enzyme, Glu233(E) and Asp197(E), respectively. These interactions mimic those made by the carbohydrate ligand and structural water molecules observed in the catalytic center [3]. This structural arrangement shows that the proteinaceous inhibitor α-AI1 targets the catalytic nucleophile [21] and its probable partners in the catalytic event.

The hydroxyl group of Tyr37(I) makes a strong hydrogen bond with Oε1 of Glu233(E), the most appropriate candidate for the role of the general acid in the first stage of the catalytic process. This tyrosine group strictly replace the water molecule (W555), present close to the point of the catalytic attack (Fig. 7), and makes an identical hydrogen-bonding pattern [3] with Glu233(E) and the chloride ligand Asn298(E) (Figs 3b,6). The hydrogen bond with Oδ1 of Asp300 is lost because, in the present complex, the aspartic acid sidechain does not rotate to adopt its functional position. Asp300 retains the conformation observed in the free enzyme and is stabilized by hydrogen bonds to the hydroxyl group of Ser189(I) and to two water molecules and a presumed Ca^{2+} ion accompanying the inhibitor. The aspartic acid sidechain sticks out into the catalytic center between the nearly parallel aromatic side-chains of Tyr37(I) and Tyr190(I).

Moving along the second inhibitor hairpin loop (L2) of α-AI1, Tyr186(I) is strongly hydrogen bonded to Oδ1 of the catalytic nucleophile Asp197(E) [21], which is located on the opposite side of the substrate binding cleft. The phenol ring of the inhibitor residue sidechain is roughly parallel to the partly planar cyclitol ring of the acarviosine moiety (Fig. 7) and its hydroxyl group mimics the O-6 oxygen atom of the cyclitol ring in the PPA–acarbose complex [3]. It is noteworthy that in the crystal structure the residue Tyr186(I) displays a conformation which falls significantly outside the energetically preferred regions of the Ramachandran diagram ([24]; Fig. 8). It is maintained in this position by the interactions described here above. In addition, its mainchain carbonyl and amine groups form hydrogen bonds with the hydroxyl group of Ser189(I), which in turn is hydrogen bonded to the carboxylic oxygen of Asp300(E).

Solvent structure

In the PPA–α-AI1 complex, most of the water molecules of the solvent network that occupy the active-site cleft in the free state of PPA are replaced by the two tyrosine residues Tyr37(I) and Tyr186(I). Only three ordered solvent molecules present in the free enzyme (W587, W643 and W748) keep their position [2] in the very central part of the

Figure 8

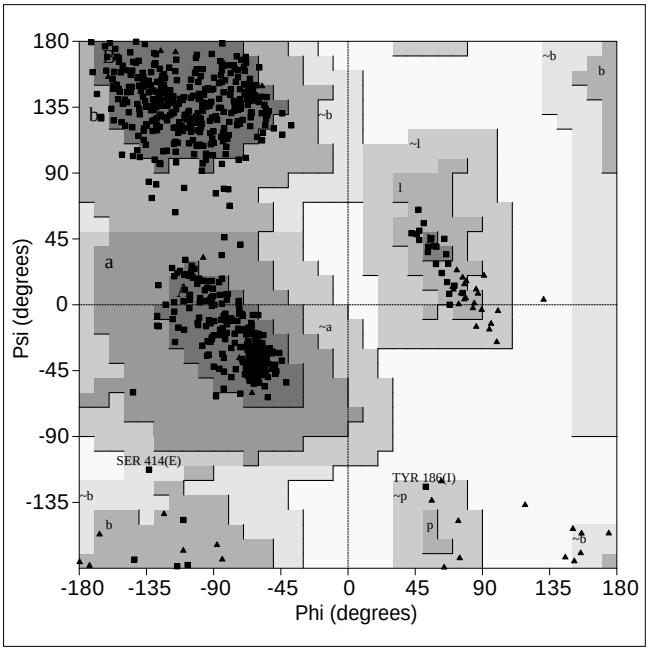

Ramachandran plot of the PPA–α-AI1 complex. (Produced with the program PROCHECK [33].) Glycine residues are shown as triangles and all other residues are squares.

catalytic cavity, between Glu233, Asp197 and Arg195. Of these, W643 appears to be the most firmly bound to the three residues (Fig. 3b). In PPA, structural water molecules W555 and W635 constitute a solvent channel that bridges across the cleft from carboxyl groups of Glu233 and Asp300 to the amide group of Asn298 (the Cl ion ligand) and the flexible loop [2,3]. In the PPA–α-AI1 complex channel this is replaced by the sidechain of Tyr37(I). As mentioned above, W555 is strictly replaced by the hydroxyl group of Tyr37(I), and W635 is replaced by a ring atom. On the other slope of the active-site depression, the part of the solvent channel found in the free enzyme that leads to bulk solvent [2] is replaced by the sidechain of Tyr186(I): its hydroxyl group substitutes W566 which was hydrogen-bonded with Oδ1 of Asp197 and the next three water molecules of the network are replaced by the tyrosine sidechain. Thus in the PPA–α-AI1 complex the central region is completely protected from the bulk solvent. The water molecule, W643, observed in both the free [2] and α-AI1-complexed PPA, is exchanged with the solvent in the PPA-acarbose complex, while W555 is close to the place of the catalytic attack [3]. In the PPA–α-AI1 complex, we observed a reversed situation, since W643 remains strongly bound to the catalytic residues while W555 is cancelled by the ligand. In the PPA–acarbose complex the catalytic center is occupied by the pseudo-disaccharide acarviosine, which is the essential structural unit responsible for the activity of all inhibitors of the acarbose type. The acarbose inhibitor (Fig. 7) gets deeper in the cleft and pushes the water molecule 643 out. W555, which was previously proposed to be the attacking nucleophile able to move to the ideal position for the nucleophilic attack at C1 [25], is conserved in all known α-amylase structures.

The structural analysis of the PPA–α-AI1 complex shows that all the important elements of the catalytic process are involved in the interaction between the enzyme and the proteinaceous inhibitor.

We have thus shown that α-AI1 inactivates PPA through an elaborate blockage of the substrate binding site on the enzyme. The stability of the complex results from an extensive set of interactions between the inhibitor and the enzyme. In particular, the inhibitor makes substrate 'mimetic' interactions with the binding subsites on the enzyme and all the catalytically competent elements of the enzyme are targeted. The hairpin loops L1 and L2 form several favourable interactions to residues that are highly conserved in the active site of α-amylases. Thus, the hairpins could serve as a template with which to design peptide-analog inhibitors. The knowledge of this inhibition mechanism is of predominant interest from the medical point of view (diabetes) and for crop protection (via plant genetic engineering).

Biological implications

Carbohydrate normally represents the majority of the human diet, and starch accounts for the major part of the 'carbohydrate pool'. Enzymatic degradation of polysaccharides is of particular significance in carbohydrate assimilation; cleavage of starch by **α**-amylases constitutes the first step of the process. The knowledge of the inhibition mechanism of **α**-amylases is of predominant interest from a medical point of view. For example, inhibition of glycolytic enzymes, especially **α**-amylases, reduces post-prandial glucose peaks, which is of particular importance in patients with diabetes.

Here we report the structure of a porcine pancreatic **α**-amylase (PPA) in complex with the bean *Phaseolus vulgaris* inhibitor (**α**-AI1). This protein inhibits the activity of both insect and mammalian **α**-amylases. Its occurrence in seeds may explain the resistance of common bean against bruchid larvae. In addition to the general interest in inhibition of glycolytic enzymes, understanding the mode of action of these proteins at the molecular level may provide an insight into the design of transgenic plants expressing either native or modified **α**-AI genes that would be resistant against some predatory insects.

Determination of the structure of the PPA–**α**-AI1 complex discloses that elements from the inhibitor molecule manage to fill the whole substrate-docking region of the PPA. They mimic the enzyme–acarbose-ligand

interactions and ligand-induced functional position of enzyme residues required for binding and/or catalysis. The catalytic nucleophile Asp197 and its probable partners located in the catalytic heart are strongly hydrogen bonded to inhibitor residues. The results show that inhibition prevents residue Asp300 from adopting its functional position and destroys the water channel leading from the 'flexible loop' to the heart of the active-site depression. This work shows how mammalian **α**-amylases and **α**-amylase inhibitors (carbohydrate-based and proteinaceous) recognize each other and how the **α**-amylases are inhibited.

Materials and methods

The structure of the PPA–α-Al1 complex was first solved at medium resolution (2.9 Å); crystallization, data collection and molecular replacement were performed as described in our previous report [14]. The crystals belong to the monoclinic space group C2, with a = 151.6 Å, b = 79.4 Å, c = 68 Å, β = 91.54° and half a complex (one inhibitor monomer and one enzyme molecule) per asymmetric unit.

Crystallization and data collection

To increase the resolution of the structure determination, new crystallization trials were carried out. The quality of the previously described crystals was improved by adding 1.8% *n*-octyl-β-D-glucopyranoside in the crystallization drop, a crystallisation reagent frequently utilized to optimize the crystal growth of macromolecules [26] (the detergent molecule is not observed in the complex structure). We obtained larger crystals (size: 0.8 × 0.5 × 0.2 mm, instead of 0.2 × 0.2 × 0.2 mm) diffracting to 1.7 Å resolution. They belong to the same space group and have identical unit cell dimensions.

Data were collected at ambient temperature from a single PPA–α-Al1 complex crystal and recorded on a 18 cm Mar-Research imaging plate scanner developed by Hendrix and Lentfer (Hamburg) on beamline X11 (l = 0.928 Å) at the EMBL Hamburg outstation. 95 frames (1° oscillation steps) were first collected between 9.0 and 1.85 Å resolution, low resolution data were taken afterwards through 38 frames (2.5° oscillation steps) collected from the same crystal, in the same orientation in the resolution range 35–4.0 Å. Data were 96.7% complete from 35–1.85 Å resolution, (Unique reflections: 66 769) and 98.4% complete from 1.92–1.85; the average overall and final shell I/σ values are 14.8 and 2.0, respectively. The merging R on intensities $\Sigma_i(\Sigma_j|I_{i,j} - \langle I_i \rangle|) / \Sigma_i \langle I_i \rangle$ was 5% (25% in the last shell). Data sets were processed with the programs DENZO and SCALEPACK [27].

Structure determination and refinement

The structure was solved by molecular replacement [14] using the program suite AMoRe [28]. The search models were the refined 2.1 Å resolution structure of PPA [2] and one monomer of the 1.9 Å resolution model of LoLI [15]. The low-resolution structure was refined to a conventional R factor of 17.6 and a R_{free} factor [29] of 29.2 in the range 8.0–2.9 Å. The overall structure of the complex was very well defined, the interactions were clearly observed in the complex structure as were two *N*-glycosylation sites and 131 water molecules. The subsequent rounds of refinement used the new sets of data and the resolution was increased to 1.85 Å.

The refinement was based on 66 557 independent reflections in the 8.0–1.85 Å resolution range and performed by simulated annealing using X-PLOR [30], followed by manual fitting into SIGMAA-weighting [31] electron-density maps with the graphics program TURBO-FRODO [32]. The procedure provided very well defined electron density for the enzyme and the inhibitor, representative $(2F_{obs}–F_{calc}) \exp(i\alpha_{calc})$ electron density corresponding to the interface of the inhibitor in the active-site region of PPA enzyme is shown in Figure 5. However some external turns in the inhibitor structure (residues 75–77; 90–95; 114–116 and 165–172) had poor or broken density. The last 19 residues at the C terminus are not seen in the electron density. The electron density enabled us to identify a third *N*-glycosylation site (five potential glycosylation sites are proposed in the literature [16]). All solvent molecules with densities below 1σ in the $(2F_{obs}–F_{calc}) \exp(i\alpha_{calc})$ map and temperature factors above 70 Å^2 were removed after the first iteration of refinement. The difference electron-density maps revealed additional water molecules. These new sites were added to the model provided that the electron density was present at a level of at least 3.5σ in the $(F_{obs}–F_{calc}) \exp(i\alpha_{calc})$ maps. The molecules introduced were inspected visually for correct geometry of hydrogen-bonding and were given an initial B factor of 20 Å^2.

In the course of analyzing the water structure, we discovered two well ordered water molecules which were in contact with six and five ligands respectively. This stereochemistry was indicative of calcium ions; the ligands may be described as lying at the vertices of tetragonal and trigonal bipyramids respectively, ~2.4 Å from the ion in the center. In addition, a water molecule was not sufficient to account for the observed density. We therefore introduced two calcium ions, which appeared consistent with the subsequent refinement procedure; their rather high B values (~40 Å^2) suggest partial occupancy of the sites, however. The B factors of the surrounding protein atoms have similar values for ligands of the presumed ion located at the enzyme–inhibitor interface, lower values (~14 Å^2) are observed for ligands from the inhibitor active site. So far, no metal ion has been identified in the bean inhibitor molecule and the unequivocal identification of the bound metal ions requires separate analysis. 325 water molecules were built into the electron density.

Quality of the final model

The final refined model yielded a conventional crystallographic R factor of 18.3% including all data from 8.0–1.85 Å and a R_{free} of 22% (the R_{free} factor was monitored separately, throughout similar refinement stages with a test set of 10% of the data). The quality of the refined structure was assessed using PROCHECK [33]. Figure 8 illustrates a Ramachandran plot [24] of the Φ/Ψ angles. All residues (except two, see below) are in allowed regions; 90.1% of the amino acid residues are in the most favoured region, only two residues (Ser114(E) [17] and Asp186(I) which are well defined in the density) are in the generously allowed region. Residue Asp186(I) is strongly hydrogen bonded to the catalytic residue Asp197(E) of the enzyme. The model has good stereochemistry (rms deviations on bond lengths, 0.010 Å; bond angles, 1.48°; and planar groups 0.03 Å). The upper estimate of the error in the atomic positions from the Luzzati plots [34] using the free R factor and a SIGMAA-plot [31] is 0.2 Å. The final model involving one enzyme molecule and the monomer unit of the inhibitor consists of 5448 protein atoms (i.e., all non-hydrogen atoms), 70 carbohydrate atoms (inhibitor *N*-glycosylation moieties), 325 water molecules, one Cl^- ion (E) and one Ca^{2+} ion (E), and two presumed Ca^{2+} ions (I). The average B factor is 23.65 Å^2 for protein atoms, (20.84 Å^2 and 24.76 Å^2 for mainchain and sidechain atoms, respectively); 45.77 Å^2 for sugar atoms and 31.47 Å^2 for solvent atoms.

Accession numbers

The atomic coordinates have been deposited at the Brookhaven Protein Data Bank (entry code 1DHK).

Acknowledgements

We are grateful to Dr Alain Roussel for assistance with program AMoRe; Drs Zbyszek Dauter, Zbyszek Otwinowski and Gideon Davies for access to the EMBL Hamburg outstation and for assistance with data collection and processing. We thank Dr Magali Mathieu for critical reading of the manuscript.

References

1. Pasero, L., Mazzei-Pierron, Y., Abadie, B., Chicheportiche, Y. & Marchis-Mouren, G. (1986). Complete amino acid sequence and location of the five disulfide bridges in protein pancreatic α-amylase. *Biochim. Biophys. Acta* **869**, 147–157.

2. Qian, M., Haser, R. & Payan, F. (1993). Structure and molecular model refinement of pig pancreatic α-amylase at 2.1 Å resolution. *J. Mol. Biol.* 231, 785–799.
3. Qian, M., Haser, R., Buisson, G., Duée, E., & Payan, F. (1994). The active center of a mammalian α-amylase. Structure of the complex of a pancreatic α-amyl with a carbohydrate inhibitor refined to 2.2 Å. *Biochemistry* 33, 6284–6294.
4. Wiegand, G., Epp, O. & Huber, R. (1995). The crystal structure of porcine pancreatic α-amylase in complex with the microbial inhibitor Tendamistat. *J. Mol. Biol.* 247, 99–110.
5. Whitaker, J.R. (1988). α-amylase inhibitors of higher plants and microorganisms. In *Food Proteins*. (Kinsella, J.E. & Soucle, W.G., eds), pp. 354–380, Proc. Prot. Co-prod. Symp., AM. Oil Chem. Soc., Campaign Il, USA.
6. Chrispeels, M.J. & Raikhel, N.V. (1991). Lectins, lectin genes, and their role in plant defense. *Plant Cell* 3, 1–9.
7. Powers, J.R. & Whitaker, J.R. (1977). Effect of several experimental parameters on combination of red kidney bean (*Phaseolus vulgaris*) α-amylase inhibitor with porcine pancreatic α-amylase. *J. Food Biochem*. 1, 239–260.
8. Schroeder, H.E., *et al*., & Higgins, T.J.V. (1995). Bean α-amylase inhibitor confers resistance to pea weevil (*Bruchus pisorum*) in transgenic peas (*Pisum sativum L*.). *Plant Physiol.* 107, 1233–1239.
9. Hoffman, L.M. & Donaldson, D.D. (1985). Characterization of two *Phaseolus vulgaris* phytohaemagglutinin genes closely linked on the chromosome. *EMBO J*. 4, 883–889.
10. Suzuki, K., Ishimoto, M. & Kitamura, K. (1994). cDNA sequence and deduced primary structure of an α-amylase inhibitor from a bruchid-resistant wild common bean. *Biochim. Biophys. Acta* 1206, 289–291.
11. Rougé, P., Barre, A., Causse, H., Chatelain, C. & Porthe, G. (1993). Arcelin and α-amylase inhibitor from the seeds of common bean *Phaseolus vulgaris* are truncated lectins. *Biochem. Syst. Ecol.* 21, 695–703.
12. Powers, J.R. & Whitaker, J.R. (1977). Purification and some physical and chemical properties of red kidney bean (*Phaseolus vulgaris*) α-amylase inhibitor. *J. Food Biochem.* 1, 217–238.
13. Pueyo, J.J., Hunt, D.C. & Chrispeels, M.J. (1993). Activation of bean (*Phaseolus vulgaris*) α-amylase inhibitor requires proteolytic processing of the proprotein. *Plant Physiology* 110, 1341–1348.
14. Gilles, C., Rousseau, P., Rougé, P. & Payan, F. (1996). Crystallization and preliminary X-ray analysis of pig pancreatic α-amylase in complex with a bean lectin-like inhibitor. *Acta Cryst. D* 52, 581–582.
15. Bourne, Y., Abergel, C., Cambillau, C., Frey, M., Rougé, P. & Fontecilla-Camps, J.C. (1990). X-ray crystal structure determination and refinement at 1.9 Å resolution of isolectin I from the seed of *Lathyrus ochrus*. *J. Mol. Biol.* 214, 571–584.
16. Marshall, J.J. & Lauda, C.M. (1975). Purification and properties of phaseolamin, an inhibitor of α-amylase from kidney bean, *Phaseolus vulgaris*. *J. Biol. Chem.* 250, 8030–8037.
17. Gilles, C., Astier, J. P., Marchis-Mouren, G., Cambillau, C. & Payan, F. (1996). Crystal structure of pig pancreatic α-amylase isoenzyme II in complex with the carbohydrate inhibitor acarbose-packing role. *Eur. J. Biochem.* 238, 561–569.
18. Strynadka, N.C.J., Jensen, S.E., Alzari, P. M. & James, M. (1996). A potent new mode of β-lactamase inhibition revealed by the 1.7 Å X-ray crystallographic structure of the TEM-1-BLIP complex. *Nat. Struct. Biol*. 3, 290–297.
19. Wilcox, E.R. & Whitaker, R. (1984). Some aspects of the mechanism of complexation of red kidney bean α-amylase inhibitor and α-amylase. *Biochemistry* 23, 1783–1791.
20. Vallee, F. (1996). Structure cristalline à 1.9 Å de resolution d'un complexe protéine–protéine entre une α-amylase d'orge et un inhibiteur bifonctionnel. Ph.D. Thesis, CNRS-Marseille & Orsay, France.
21. McCarter, J.D. & Withers, S.G. (1996). Unequivocal identification of Asp214 as the catalytic nucleophile of *Saccharomyces cerevisiae* α-glucosidase using 5-fluoro glycosil fluorides. *J. Biol. Chem.* 271, 6889–6894.
22. Mirkov, T.E., Evans, S.V., Wahlstrom, J., Gomez, L., Young, N.M. & Chrispeels, M.J. (1995). Location of the active site of the bean α-amylase inhibitor and involvement of a Trp, Arg, Tyr triad. *Glycobiology* 5, 45–50.
23. Higgins, T.J.V., Chandler, P.M., Zurawaski, G., Button, S.C. & Spencer, D. (1983). The synthesis and primary structure of pea seed lectin. *J. Biol. Chem.* 258, 9544–9549.
24. Ramachandran, G.N. & Sasisekharan, V. (1968). Conformation of polypeptides and proteins. *Adv. Protein Chem*. 23, 283–437.
25. Mazur, A.K., Haser, R. & Payan, F. (1994). The catalytic mechanism of α-amylases based upon enzyme crystal structures and model building calculations. *Biochem. Biophys. Res. Commun.* 204, 297–302.
26. Cudney, B., Patel, S., Weisgraber, K., Newhouse, Y. & McPherson, A. (1994). Screening and optimization strategies for macromolecular crystal growth. *Acta Cryst. D* 50, 414–423.
27. Otwinowski, Z. (1993). Oscillation Data Reduction Program. In *Proceedings of the CCP4 Study Weekend*: *Data Collection and processing*. (Sawyer, L., Isaacs, N. & Burley, S., eds), pp. 56–62, Daresbury Laboratory, Warrington, UK.
28. Navaza, J. (1994). AMoRe: an automated package for molecular replacement. *Acta Cryst. A* 50, 157–163.
29. Brünger, A.T. (1992). Free R value: a novel statistical quantity for assessing the accuracy of crystal structures. *Nature* 355, 472–475.
30. Brünger, A.T. (1992). *X-PLOR, Version 3.1. A system for X-ray Crystallography and NMR*. Yale University Press, New Haven, CT.
31. Read, R.J. (1986). Improved Fourier coefficients for maps using phase from partial structure with errors. *Acta Cryst. A* 42, 140–149.
32. Roussel, A. & Cambillau, C. (1992). TURBO-FRODO, Biographics and AFMB (Architecture et Fonction des Macromolécules Biologiques), Marseille, France.
33. Laskowski, R.A., MacArthur, M.W., Moss, D.S. & Thornton, J.M. (1993). PROCHECK: a program to check the stereochemistry of protein structures. *J. Appl. Cryst.* 26, 283–291.
34. Luzzatti, P.V. (1952). Traitement statistique des erreurs dans la determination des structures cristallines. *Acta Cryst.* 5, 802–810.
35. Nicholls, A.J. (1993). GRASP manual. Graphical representation and analysis of surface properties. Columbia University, NY, USA.